

A Three-Dimensional Atom Probe Microscope Incorporating a Wavelength-Tuneable Femtosecond-Pulsed Coherent Extreme Ultraviolet Light Source

Ann N. Chiamonti¹, Luis Miaja-Avila¹, Paul T. Blanchard¹, David R. Diercks², Brian P. Gorman², and Norman A. Sanford¹

¹National Institute of Standards and Technology, Boulder, CO, USA

²Colorado School of Mines, Golden, CO, USA

ABSTRACT

Pulsed coherent extreme ultraviolet (EUV) radiation is a potential alternative to pulsed near-ultraviolet (NUV) wavelengths for atom probe tomography. EUV radiation has the benefit of high absorption within the first few nm of the sample surface for elements across the entire periodic table. In addition, EUV radiation may also offer athermal field ion emission pathways through direct photoionization or core-hole Auger decay processes, which are not possible with the (much lower) photon energies used in conventional NUV laser-pulsed atom probe. We report preliminary results from what we believe to be the world's first EUV radiation-pulsed atom probe microscope. The instrument consists of a femtosecond-pulsed, coherent EUV radiation source interfaced to a local electrode atom probe tomograph by means of a vacuum manifold beamline. EUV photon-assisted field ion emission (of substrate atoms) has been demonstrated on various insulating, semiconducting, and metallic specimens. Select examples are shown.

INTRODUCTION

Three-dimensional (3D) atom probe tomography (APT) is an isotopically-sensitive analytical technique that can provide unique information on the composition and structure of nanoscale interfaces. Unlike other interfacial characterization techniques (e.g. scanning and conventional transmission electron microscopy, electron energy loss spectrometry, secondary ion mass spectrometry, ellipsometry) APT offers the desirable

combination of both high spatial resolution (< 0.2 nm lateral and < 0.1 nm in depth) [1] and high analytical sensitivity (approaching the ppm range) across the entire periodic table. APT does not require the interfaces of interest in the specimen to be aligned in any particular direction relative to an optic axis, zone axis, or any special analysis direction and significantly, APT measurements do not average through specimen thickness. Analysis of the data can provide information on the physical and chemical roughness of buried, arbitrarily shaped and oriented interfaces through the calculation of isoconcentration surfaces or proximity histograms [2-4]. Finally, APT can make quantitative measurements and two-dimensional maps of the Gibbs interfacial excess, which is an important thermodynamic quantity that indicates the amount of substance enriched or depleted at an interface per unit area [2].

Conventional NUV laser-pulsed APT works on the basis of field ion evaporation. In this process, the thermal transient resulting from a near ultraviolet (NUV) laser pulse incident upon the specimen triggers an atom from the specimen surface to field evaporate as an ion [5]. As shown in Figure 1, the specimen is electrically biased relative to a counter

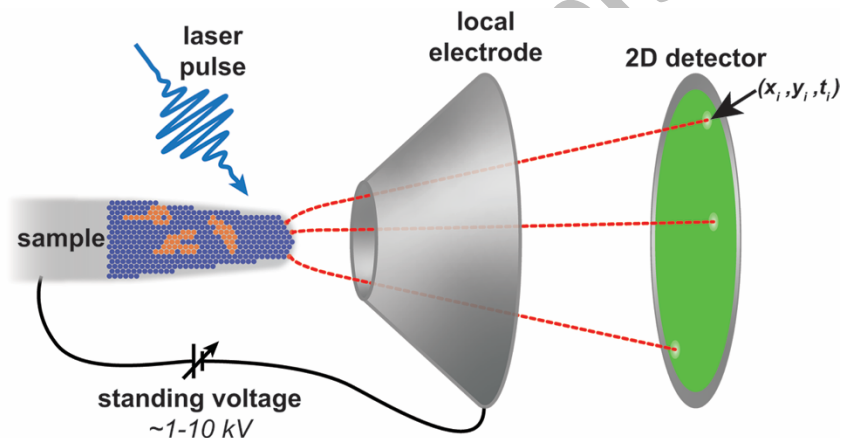


Figure 1: Schematic of the APT process. In conventional laser-pulsed APT, a sharp needle-shaped specimen is biased relative to a conical counter electrode. The bias (standing) voltage induces a surface electric field that is typically ≈ 10 V/nm (on the vacuum side of the tip-vacuum interface). The voltage is held just under the threshold for field ion evaporation of a given material. The thermal transient imparted to the specimen from a pulsed NUV laser triggers field ion evaporation of individual specimen atoms or cluster molecules. The atoms field evaporate as ions, and accelerate under the standing voltage toward a position-sensitive, delay-line detector where an event is detected in 2D space (x_i, y_i) . The time of the ionization event is correlated with the laser trigger pulse and the isotopic identity of the atom or molecular cluster can be deduced from its flight time (t_i) and analysis of the mass spectrum. In the analysis of APT data, the specimen is essentially “deconstructed” one atom at a time and then virtually “reconstructed” in software. The physical locations of the atoms in the original specimen are calculated from a combination of the impact coordinates on the 2D detector and back projection/sequential fill algorithms [6-8]. The resulting 3D dataset is a sub-nm spatially resolved model of the atoms in the original specimen. (Figure courtesy of Benjamin W. Caplins, NIST)

electrode such that the induced surface electric field at the apex (in vacuum) is on the order of 10 V/nm to 50 V/nm. This serves to both lower the activation energy barrier for thermal field ion emission and accelerate the evaporated ion toward a two-dimensional (2D) position-sensitive, time-of-flight (ToF) detector. The isotopic identity of the ion can be inferred from its flight time and analysis of the mass spectrum, and its location in the original sample can be inferred by combining the location where it hit the detector with back projection/sequential fill methods [6-8]. Ideally, the result is a 3D “reconstructed” image where each detection event represents a spatially- and isotopically-resolved atom or molecule evaporated from the original specimen. Conventional laser-pulsed APT has been used to analyse many types of materials ranging from metals, semiconductors, and insulators to polymers, biological materials, and recently even frozen liquids [9]. APT has proven quite valuable when applied to problems in high performance alloys, materials for energy production and storage, microelectronics, geology, nuclear storage, corrosion, biological implants, and many more.

As powerful as APT has proven to be, the measurements can sometimes suffer from various shortcomings and artifacts, which can lead to increased uncertainty and error in composition measurements. In addition to the fundamental issue that some materials suffer poor absorption in the near ultraviolet band, such complications often arise from the fundamental physical mechanisms that define the thermally-activated, field ion evaporation process itself. Laser pulsing of field evaporation can cause thermal artifacts in many materials, and is particularly problematic in complex heterogeneous materials that have discontinuities in optical absorption, evaporation field, and thermal conductivity. Other sources of uncertainty and error are the formation of cluster or molecular ions. Cluster ion evaporation can lead to isobaric (mass spectral peak) overlaps that increase the uncertainty in composition measurements. For example, the cluster ion $^{12}\text{C}_2^{++}$ containing 2 carbon atoms overlaps at 12 Da with the ion $^{12}\text{C}^+$ that containing only 1 carbon. Isobaric overlaps such as these can sometimes be resolved by analysis of the expected isotopic ratios; in other cases, they cannot be distinguished and this increases the uncertainty of composition measurements. Evaporation of molecular ions is also undesirable because it degrades the spatial resolution of a reconstruction since an entire complex of atoms is mapped to a single voxel. Multiple, simultaneous ion hits on the detector (also known as ion pile-up or “multi-hits”) increase uncertainty and measurement error when they cannot be resolved to their constituent atoms or molecules. This results in a loss of information in general, and is particularly problematic for some covalent and ionically bonded materials as well as some individual atomic species (e.g. the C in steel) that preferentially evaporate as multiple hits [10,11]. Finally, persistent evaporation of ions (so-called “thermal tails”) following a laser pulse increases uncertainty and degrades APT performance by decreasing mass resolving power and potentially obscuring the mass spectral peaks from dilute species.

Our early results show that pulsed coherent extreme ultraviolet (EUV) radiation ($10 \text{ eV} \leq E \leq 100 \text{ eV}$; $124 \text{ nm} \geq \lambda \geq 12 \text{ nm}$) is a potential alternative to pulsed NUV laser radiation sources for triggering substrate atom field ion emission that is necessary to perform APT. EUV photon energies can be selected to be above the optical absorption edge, work function, and ionization potential of any material. Optical absorption is generally within the first few nanometers of the surface, and photoionization cross-sections peak in the EUV band across the periodic table. More importantly, EUV radiation may offer potentially *athermal* ionization mechanisms through direct photoionization or core-

hole Auger decay [12,13] that are not possible at the lower photon energies employed in conventional laser-pulsed APT.

One should not confuse our work, which is exclusively associated with coherent pulsed EUV radiation sources applied to *substrate atom* field ion emission required for 3D atom probe microscopy, with prior reports of EUV radiation used in the context of field ion microscopy. Photon-assisted field ionization (ionization of an imaging gas on or above a field emitter surface) and photon-assisted adsorbate field desorption (ionization of an adsorbed gas on a field emitter surface) using pulsed EUV synchrotron radiation have been successfully demonstrated in the past [14-17]. However, none of these studies demonstrated EUV radiation-triggered field ion emission of substrate atoms themselves. Therefore, the results we present herein are distinct and new to the best of our knowledge.

EXPERIMENTAL DETAILS

The NIST EUV APT (Figure 2) was constructed by combining a femtosecond-pulsed coherent EUV light source with a straight flight path atom probe tomograph [18,19]. As EUV radiation is strongly absorbed in ambient air, the photon source and APT chamber are linked with a high-vacuum manifold beamline.

Femtosecond-Pulsed Coherent EUV Photon Source

Femtosecond-pulsed, coherent EUV light in the NIST EUV APT is produced by means of high harmonic generation (HHG). HHG is a nonlinear process where an ultrafast driving laser pulse (referred to as the “fundamental”) incident upon a noble gas in a hollow-core capillary waveguide produces odd-order harmonics of the fundamental (optical) frequency [20,21]. EUV photons produced through HHG are strongly coupled to the field of the driving laser and form a coherent EUV beam. Available EUV photon energies generally range from ≈ 10 eV, when using Kr or Xe, to ≈ 40 eV for Ar, and up to ≈ 100 eV when using He or Ne [22]. One should bear in mind that the exact EUV range available for a given noble gas depends on the wavelength of the driving laser; for the work presented herein, an 800 nm (infrared) driving laser was used.

In our approach, the driving laser pulses are derived from an amplified Ti:Sapphire laser system (Wyvern, KM Labs, Boulder, CO)* that delivers 0.5 mJ per pulse at a repetition rate of 10 kHz with a pulse duration of ≈ 35 fs. This is focused coaxially into the HHG capillary, where the EUV photons are generated (XUUS, KM Labs, Boulder, CO). The resulting EUV output depends on many parameters including the capillary length and diameter, the laser pulse duration, and the specie and pressure of the noble gas used.

Ar gas was chosen to be the HHG media for our initial experiments. In our configuration, the peak intensity occurs approximately near the 27th to the 29th harmonic of the fundamental, yielding EUV photons that have an energy of approximately 41.85 eV to 44.95 eV (wavelength of 29.6 nm to 27.6 nm). Interestingly, the EUV pulse width is assumed to be less than 10 fs based on measurements from similarly configured systems

[23]. In our system, the EUV pulse energy was measured to be 0.5 pJ at the sample position.

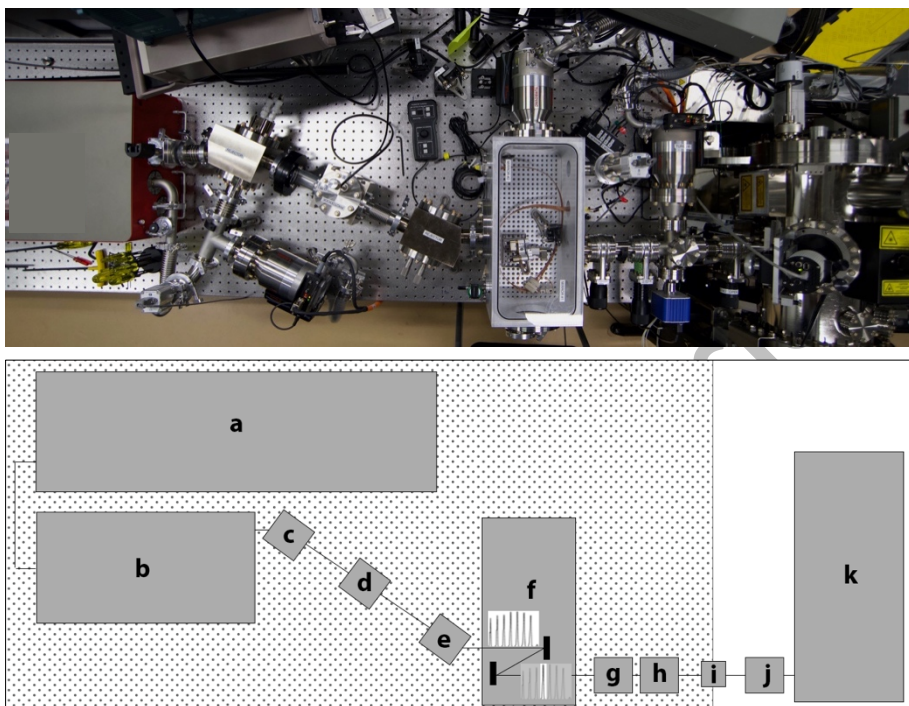


Figure 2: Photograph (top) and schematic drawing (bottom) of the NIST extreme ultraviolet radiation-triggered atom probe tomograph. The coherent EUV source consists of (a) an amplified Ti:sapphire laser and (b) high harmonic generation module that contains the hollow-core capillary waveguide. The vacuum manifold (c-j) consists of the following components: (c) first infrared light rejecting filter, (d) photodiode, (e) second infrared light rejecting filter (f) vacuum chamber containing the EUV optics, (g,h) UHV gate valves containing filters to block either the fundamental frequency or the EUV harmonics present in the beam, (i) vacuum bellows for vibration isolation, and finally (j) a standard UHV gate valve. The APT chamber is labelled (k). Several turbomolecular pumps and vacuum gauges are present in the photograph but not represented on the schematic.

† Identification of specific commercial products or vendors is intended only to adequately describe the experimental conditions. This does not imply endorsement by the National Institute of Standards and Technology. Other vendors, products, or services may be adequate or superior alternatives.

Vacuum Manifold Beamline

EUV radiation is strongly attenuated in air necessitating the use of an evacuated beam path, achieved by means of a vacuum manifold connecting the output of the HHG capillary (pressure $\approx 5 \times 10^3$ Pa (40 Torr)) with the atom probe tomograph analysis chamber (pressure $\approx 2.6 \times 10^{-9}$ Pa (2×10^{-11} Torr)). Pressure differentials along the

beamline are achieved by means of three turbomolecular pumps, as discussed below. In addition to acting as a differential pumping manifold, the beamline also contains several elements necessary to focus and steer the EUV beam at the specimen location as well as measure the properties of the EUV source.

Since the EUV and the driving laser co-propagate out of the HHG capillary, rejector mirrors consisting of Si wafers mounted at approximately Brewster's angle (for infrared light) are utilized to attenuate the fundamental. Each rejector absorbs $\approx 80\%$ of the fundamental while reflecting $\approx 80\%$ of the EUV [24]. The first turbomolecular pump is mounted on the first rejector mirror housing, and pressures of 10^{-3} Pa (10^{-5} Torr) are achieved in this section of the beamline.

Following the rejectors is a small, subsidiary vacuum chamber containing steering and focusing optics. The second turbomolecular pump is mounted to this chamber. The pressure is maintained at a base level of 10^{-5} Pa ($\approx 10^{-7}$ Torr) when the beamline is isolated and rises to roughly 10^{-3} Pa ($\approx 10^{-5}$ Torr) when the beamline is open to the coherent EUV source. For the initial experiments, multilayer mirrors were chosen (rather than toroidal or ellipsoidal mirrors) for their convenience in focusing and steering the beam. The multilayer mirrors operate as a band-pass filter for a single harmonic. The optics currently used in the EUV APT were designed to reflect only the 27th harmonic of the fundamental ($E = 41.85$ eV; $\lambda = 29.6$ nm) with a bandwidth of ≈ 2.8 eV.

The last elements in the beamline before the UHV APT analysis chamber are a series of UHV-compatible, bakeable gate valves. In two of the valves, the stainless steel gates are replaced with filter (solid) windows that serve two purposes: to pass or block specific spectral components of the beam and to help maintain vacuum differentials. One gate valve effectively blocks the EUV photons but allows the weak, residual 800 nm light to pass. The second gate valve/filter contains an Al film that blocks the remaining 800 nm light but has approximately 80 % transmissivity for ≈ 40 eV photons [24]. Following the two filter gate valves is the third turbomolecular pump; the pressure in this area of the beamline is $\approx 10^{-7}$ Pa ($\approx 10^{-9}$ Torr). A vacuum bellows is used for vibration isolation between the laser table and the APT chamber, and one final UHV gate valve isolates the beamline on the analysis chamber side when the system is idle. The pressure maintained in the APT analysis chamber during data acquisition is typically $\approx 2.6 \times 10^{-9}$ Pa (2×10^{-11} Torr).

Atom Probe Chamber

The atom probe chamber in the NIST EUV APT is a LEAP 3000X-Si local-electrode straight flight path atom probe tomograph (CAMECA Instruments, Madison, WI). This instrument originally came equipped with a 532 nm (green) laser, which was removed for our experiments. The only modification of this instrument from its commercial form is that the EUV laser is introduced through the 0° port antiparallel to the puck transfer arm. This port formerly contained a so-called low-resolution "puck loading camera" that is no longer in use. Otherwise, the APT chamber is operated in the normal way, that is to say specimens are inserted via a load lock and introduced to the UHV analysis chamber through an intermediary buffer chamber. Conveniently, the LEAP 3000 tool uses an analog time-to-digital convertor (TDC) that can be triggered by an external source, in our case, from a fast photodiode that picks-off a small portion of the 800 nm driving laser. The TDC enables ToF measurements; it converts a series of start and event timing pulses into a time-correlated histogram of detection events (i.e. the ToF spectrum).

It tells the instrument when to “start counting” in preparation for the laser or EUV photon pulse that will follow. Since EUV photons (in addition to ions and electrons) can be detected on the multi-channel plate detector, the value of t_0 (i.e. “time zero”, the basis from which ion flight times are calculated and what is used for mass calibration) is approximately determined by noting the time when the scattered primary EUV photon beam hits the detector. Therefore, we exploit stray EUV light to our advantage – rather than worry it will corrupt our data.

For the prototype configuration of the EUV APT, it was not necessary to build active focus and steering feedback control of the EUV beam. This subtle point deserves more clarification as follows. The multilayer mirror optics yield a focused EUV spot diameter of $\approx 50 \mu\text{m}$ at the specimen tip, as determined by means of an X-ray phosphor ($\text{Gd}_2\text{SO}_4:\text{Tb}$) that temporarily replaces the specimen. Pointing (x,y) of the EUV beam is adjusted manually to maximize the ion detection rate, and manual adjustments may be periodically updated during the course of data acquisition. Of course, we plan future improvements that will incorporate both active beam-steering control, and tighter focus of the EUV at the specimen location.

Sample Preparation for EUV APT

Specimens were prepared from samples using conventional methods for a given material type. Metal specimens were in the form of a long (≈ 0.5 cm) electropolished wire of the sample material; Sb-doped Si specimens are commercially-available, lithographically-patterned, pre-sharpened micro-post array coupons (CAMECA Instruments, Madison, WI). The remaining specimens were prepared by standard focused ion beam (FIB) lift-out procedures [25]. The only manner in which our FIB-prepared specimens differ from those that would be used in a conventional laser-pulsed APT is that we account for the large physical EUV beam spot size in our proof-of-principle instrument by sharpening them so that the tips stand at least $50 \mu\text{m}$ higher than the substrate, nearby spires, or any other surrounding features.

RESULTS AND DISCUSSION

EUV radiation-pulsed APT data has been successfully obtained from several material classes to date including both crystalline and amorphous materials. These include insulators (e.g. SiO_2 , BaTiO_3), semiconductors (GaN , GaN:Mg , InGaN , AlGaN , Si), and a metal (Al). For brevity, one example from each type of material is shown in Figure 3.

Examples

All of the EUV APT data shown here was collected at 0.5 pJ pulse energy, 10 kHz pulse rate, and 50 K base temperature. A mass spectrum from an amorphous SiO_2 specimen is shown in Figure 3(a). An estimate of the time-independent background is shown in red, and the background corrected mass spectrum is displayed in Figure 3(b).

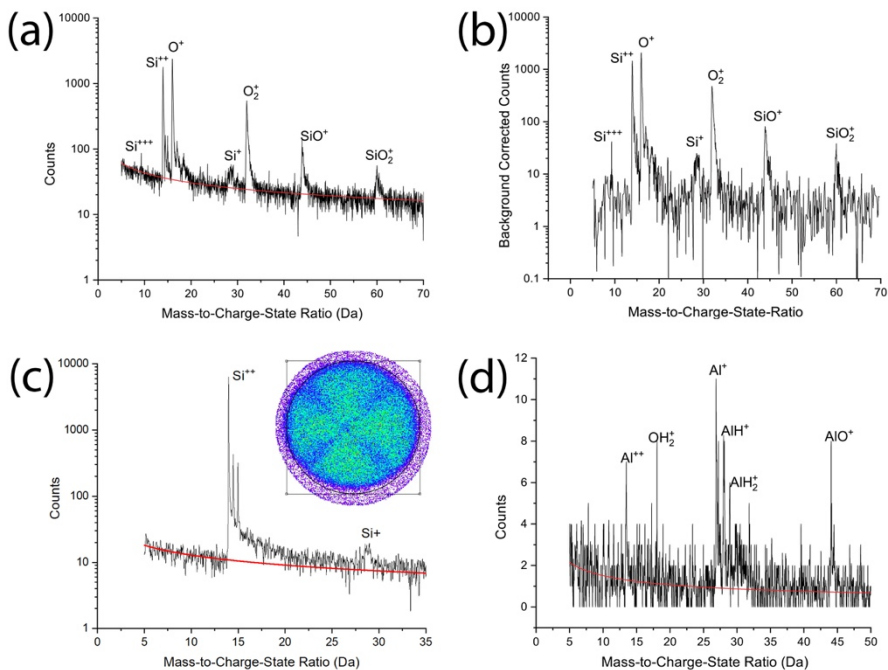


Figure 3: EUV APT data. All data were collected at 0.5 pJ pulse energy, 10 kHz pulse rate, and at a base temperature of 50 K. The display bin size is 30 mDa. Estimates of the time-independent background are displayed as a solid line (colored red in the online version) overlaying the data (a) Uncorrected mass spectrum from an amorphous SiO_2 specimen. (b) Time-independent background-corrected mass spectrum from the SiO_2 data in (a). (c) Uncorrected mass spectrum from $\langle 100 \rangle$ -oriented single crystal silicon. (Inset, c) Desorption map (detector event histogram) from a single crystal Si specimen. (d) Uncorrected mass spectrum from an electropolished Al wire (with native oxide).

Figure 3(c) shows a mass spectrum and desorption map (detector event histogram) from a commercially-available, lithographically-patterned, single-crystal silicon specimen. As in NUV APT, we observed the 4-fold symmetry of the $\langle 100 \rangle$ crystallographic pole as a cross-shaped region of low hit density on the detector event histogram (“hitmap”) and in the reconstructed data for this crystalline specimen. Such features are the result of trajectory aberrations at poles and along zone lines in crystalline samples [26].

The mass spectrum from an electropolished Al wire is shown in Figure 3(d). Data from the Al wire were difficult to obtain in the EUV system and the total ranged ion counts are comparatively low. One possibility for this difficulty in obtaining data from this metal sample is that the data collection rate was limited by the EUV fluence. In other words, a higher EUV laser pulse energy per unit area may be required to effectively ionize and desorb some metals under EUV illumination. The standing voltage for the Al sample was held just below the threshold for DC field evaporation. Increasing the standing voltage did not increase the rate of evaporation of specimen ions; instead, it simply increased the time-

independent evaporation events (manifested as background noise). Another possibility for the difficulty in obtaining EUV data on the metal sample shown here is that ionization is via an athermal process and the ion is neutralized before it can desorb, as discussed by Tsong in reference to photoexcitation in the field ion microscope [27], and others, within the context of electron stimulated desorption [28]. As the laser pulse energy in the EUV APT is fixed in this prototype instrument, testing these hypotheses are goals of future work. Nevertheless, the expected peaks are present in the mass spectrum and correspond to Al metal, Al hydrides, AlO (from the native oxide layer), and water (from the vacuum chamber).

SUMMARY AND FUTURE WORK

To the best of our knowledge, we have designed, built, and demonstrated operation of the first extreme ultraviolet radiation-triggered atom probe microscope. This instrument uses femtosecond-pulsed, coherent EUV photons from high harmonic generation (HHG) in a noble gas-filled hollow-core capillary waveguide to trigger field-assisted ion emission from an electrically biased specimen. This paper describes the basics of the instrument design including the EUV source, the vacuum manifold, optics, and the atom probe chamber. EUV photon-triggered substrate atom field ion emission was demonstrated on a variety of samples, and select preliminary results are shown.

Plans underway to further develop the EUV APT capability include: replacing the driving laser with one that operates at a higher repetition rate, improving the focusing optics to obtain higher EUV fluence at the specimen location, active evaporation-rate feedback for EUV beam steering control, and integrated electron optics for real-time, in situ specimen shape imaging. Future work aims to understand the ionization and evaporation processes that occurs on a specimen surface under the simultaneous influences of high DC electric field and femtosecond-pulsed EUV illumination. This will be pursued in part by exploiting the tunability of the EUV source as afforded by the use of different noble gasses in the HHG capillary.

The EUV photon energy used is above the bandgap, work function, and even the ionization potential of nearly any element; this is not true for NUV wavelengths. Consequently, EUV affords potential ionization and desorption pathways *in addition to, or working in combination with, thermal pulsing of field evaporation*. These additional pathways and mechanisms, which have never been conclusively demonstrated in conventional laser-pulsed APT, include photoexcitation, photoionization, or Auger decay. Finally, we underscore key findings of this work: namely, useful field ion emissions yields are obtained, and stoichiometry can be recovered, in spite of the fact that the EUV photon fluence (J/cm^2) incident on the specimen tip is *orders of magnitude lower* than that used in a conventional, NUV laser-pulsed atom probe tomograph operating at comparable standing voltages.

ACKNOWLEDGMENTS

This project received funding through the NIST Innovations in Measurement Science Program. Material support was provided from CAMECA Instruments, Inc.

through a cooperative research and development agreement. Administrative and technical leadership from K.B. Rochford, M.L. Dowell, and T.F. Kelly were instrumental in launching the project. D.D. Hickstein and J.L. Ellis helped with the design of the EUV beamline.

REFERENCES

1. E. Cadel, F. Vurpillot, R. Larde, S. Duguay, and B. Deconihout. *J. Appl. Phys.* **106** 044908 (2009).
2. Hellman, J.A. Vandenbroucke, J. Rusing, D. Ishiem, and D.N. Seidman. *Microsc. Microanal.* **6**, 437 (2000).
3. B. Gault, M.P. Moody, J.M. Cairney, and S.P. Ringer. *Atom Probe Microscopy* (Springer, New York, 2012).
4. D.J. Larson, T.J. Prosa, R.M. Ulfing, B.P. Geiser, and T.F. Kelly. *Local Electrode Atom Probe Tomography* (Springer, New York, 2013).
5. T.T. Tsong. *Atom-Probe Field Ion Microscopy* (Cambridge University Press, Cambridge, 1990).
6. D. Blavette, J.M. Sarrau, A. Bostel, and J. Gallot. *Rev. Phys. Appl.* **17** 435 (1982).
7. P. Bas, A. Bostel, B. Deconihout, and D. Blavette. *Appl. Surf. Sci.* **87-88** 298 (1995).
8. B.P. Geiser, D.J. Larson, E. Oltman, S. Gerstl, D. Reinhard, T.F. Kelly, and T.J. Prosa. *Microsc. Microanal.* **15 S2** 292 (2009).
9. S.S.A. Gerstl, S. Tacke, Y-S. Chen, J. Wagner, and R. Wepf. *Microsc. Microanal.* **23** 612 (2017).
10. G. Da Costa, H. Wang, S. Suguay, A. Bostel, D. Blavette, and B. Deconihout. *Rev. Sci. Inst.* **83** 123709 (2012).
11. F. Meisenkothen, E.B. Steel, T.J. Prosa, K.T Henry, and R. P. Kolli. *Ultramicroscopy* **159** 101 (2015).
12. M.L. Knotek and P.J. Feibelman. *Phys. Rev. Lett.* **40** 964 (1978).
13. M.L. Knotek, V.O. Jones, and V. Rehm. *Phys. Rev. Lett.* **43** 300 (1979).
14. S. Jaenicke, A. Ciszewski, W. Drachsel, U. Weigmann, T.T. Tsong, J. Pitts, J. Block, and D. Menzel. *J. Phys. Coll.* **47** C7:343 (1986).
15. W. Weigmann, S. Jaenicke, R. Pitts, W. Drachsel and J.H. Block. *J. Phys. Coll* **47** C2:145 (1986).
16. W. Drachsel, S. Jaenicke, A. Ciszewski, J. Dosselmann, and J.H. Block. *J. Phys. Coll* **48** C6:227 (1987).
17. S. Jaenicke, J. Dosselmann, A. Ciszewski, W. Drachsel, and J.H. Block. *Surf. Sci.* **211** 804 (1989).
18. N.A. Sanford, A.N. Chiamonti Debay, B.P. Gorman, and D.R. Diercks. U.S. Patent No 9 899 197 (20 February, 2018).
19. N.A. Sanford and A. Chiamonti Debay. U.S. Patent No 10 153 144 (11 December, 2018).

20. A. Rundquist, C.G. Durfee III, Z. Chang, K. Herne, S. Backus, M.M. Murnane, and H.C. Kapteyn. *Science* **280** 1412 (1998).
21. J. Wildenauer. *J. Appl. Phys.* **62** 41 (1987).
22. G. Cirimi, C.-J. Lai, E. Granados, S.-W. Huang, A. Sell, K.-H. Hong, J. Moses, P. Keathley, and F.X. Kartner. *J. Phys. B: At. Mol. Opt. Phys.* **45** 205601 (2012).
23. L. Miaja-Avila, C. Lei, M. Aeschlimann, J.L. Gland, M.M. Murnane, H.C. Kapteyn, and G. Saathoff. *Phys. Rev. Lett.* **97** 113604 (2006).
24. Lawrence Berkeley National Laboratory Center for X-Ray Optics. X-Ray Interactions with Matter Filter Transmission Calculator. www.henke.lbl.gov/optical_constants/filter2.html. Accessed 20 March 2019.
25. K. Thompson, D. Lawrence, D.J. Larson, J.D. Olson, T.F. Kelly, and B.P. Gorman. *Ultramicroscopy* **107** 131-129 (2007).
26. A.R. Waugh, E.D. Boyes, and M.J. Southon. *Surf. Sci.* **61** 109 (1976).
27. T.T. Tsong, J.H. Block, M. Nagasaka, and B. Viswanathan. *J. Chem. Phys.* **65** 2469 (1976).
28. J. Dirks, W. Drachsel, and J.H. Block. *Appl. Surf. Sci.* **67** 118 (1993).